ACS MATERIALS Au
AN OPEN ACCESS JOURNAL OF THE AMERICAN CHEMICAL SOCIETY

pubs.acs.org/materialsau
Letter

Cell-Sized Confinements Alter Molecular Diffusion in Concentrated Polymer Solutions Due to Length-Dependent Wetting of Polymers

Yuki Kanakubo, Chiho Watanabe, Johtaro Yamamoto, Naoya Yanagisawa, Hiroki Sakuta, Arash Nikoubashman,* and Miho Yanagisawa*

Cite This: ACS Mater. Au 2023, 3, 442–449
Read Online

ACCESS | Metrics & More | Article Recommendations | Supporting Information

ABSTRACT: Living cells are characterized by the micrometric confinement of various macromolecules at high concentrations. Using droplets containing binary polymer blends as artificial cells, we previously showed that cell-sized confinement causes phase separation of the binary polymer solutions because of the length-dependent wetting of the polymers. Here, we demonstrate that the confinement-induced heterogeneity of polymers also emerges in single-component polymer solutions. The resulting structural heterogeneity also leads to a slower transport of small molecules at the center of cell-sized droplets than that in bulk solutions. Coarse-grained molecular simulations support this confinement-induced heterogeneous distribution by polymer length and demonstrate that the effective wetting of the shorter chains at the droplet surface originates from the length-dependent conformational entropy. Our results suggest that cell-sized confinement functions as a structural regulator for polydisperse polymer solutions that specifically manipulates the diffusion of molecules, particularly those with sizes close to the correlation length of the polymer chains.

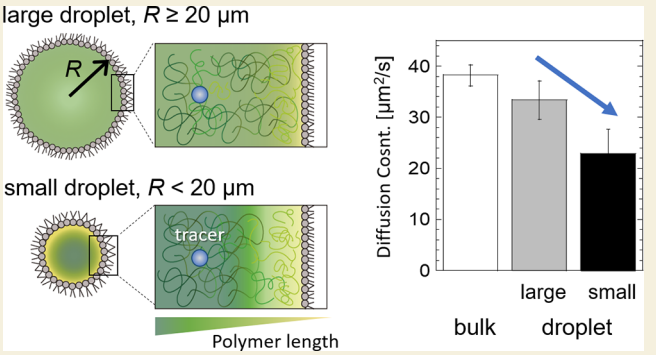

KEYWORDS: *macromolecular crowding, artificial cell, depletion effect, FCS, fluorescence correlation spectroscopy, molecular simulation*

The cytoplasm of living cells typically contains numerous (macro)molecular components at high concentrations.[1,2] These components cover a wide size spectrum, ranging from a few nanometers in single proteins to several micrometers in cytoskeletal filaments. The positioning of these components within the cell is strongly tied to their biological functions; e.g., the long-lived cytoskeleton formed by intermediate filaments beneath the cell membrane exhibits strain stiffening in response to an external load, thereby protecting cells from harmful deformations.[3] The identity and concentration of the (macro) molecular components can be analyzed from the fluorescence labeling of target molecules[4] and measurements of local physical properties, such as the refractive index (RI),[5] polarization,[6] and absorption efficiency of light.[7,8]

Recently, the dynamic formation of biomolecular condensates through liquid–liquid phase separation (LLPS) has attracted attention as a mechanism to regulate the dynamic positioning of molecules. For example, in an in vitro system, Monterroso et al. demonstrated that LLPS can modulate the assembly of the protein FtsZ, which plays a key role in bacterial cell division.[9] From a polymer physics perspective, the formation and positioning of biomolecular condensates depend on many factors, including molecular properties (e.g., the sequences of RNA nucleotides and protein amino acids), molecular concentration, and solution conditions (e.g., temperature, pH, and salinity), which have been extensively studied through experiments and simulations.[10,11] An important but frequently overlooked property is molecular length. However, it is challenging to characterize the length distribution of molecules inside and outside the biomolecular condensates owing to difficulties in multifluorescent labeling by length. Furthermore, physical quantities, such as RI, are less sensitive to the molecular length than to the concentration (see a case study on dextran solutions[12]).

Recently, we demonstrated that such heterogeneous distributions by polymer length can become particularly prominent for binary polymer solutions confined in cell-sized water-in-oil (W/O) droplets covered with a lipid membrane.[13,14] Experiments and simulations have revealed that shorter polymers have a higher membrane wettability, which in turn, enhances the localization of short/long polymers at the surface/center of the droplets. This results in LLPS at concentrations where bulk systems would still be in the fully

Received: March 10, 2023
Revised: May 8, 2023
Accepted: May 10, 2023
Published: May 16, 2023

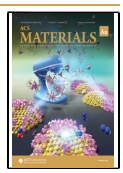

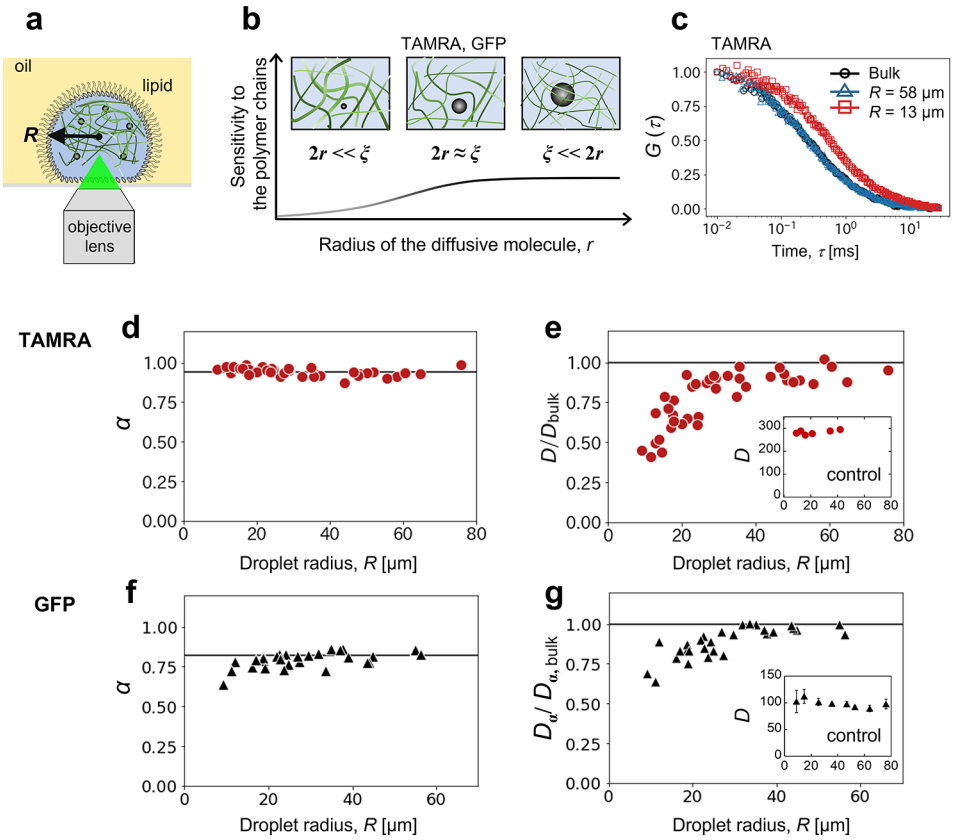

Figure 1. (a) Schematic of the FCS experiment for dextran PC droplets. (b) Illustration of the sensitivity of diffusive molecules to the polymer chains against the size ratio between the polymer mesh size, ξ, and diameter of the tracer molecule, $2r$. (c) ACFs of TAMRA diffusion inside droplets containing 400 mg/mL Dex150k (squares and triangles) and in the corresponding bulk (black circles). The values are normalized at 10^{-2} ms. The droplet radius, R, is 58 μm (blue triangles) and 13 μm (red squares). The bulk ACF (black circles) is practically identical with the ACF of the large droplet (blue triangles). (d–g) R-dependent diffusion inside droplets containing 400 mg/mL Dex150k for (d, e) TAMRA ($2r/\xi \approx 0.7$–0.9) and (f, g) GFP ($2r/\xi \approx 2.3$–2.9). (d, f) Anomalous exponent α and (e, g) normalized diffusion coefficient D/D_{bulk} is plotted against R. Their bulk values are (d) $\alpha_{bulk} = 0.94 \pm 0.02$ (Ave. ± S.D., $N = 25$); (e) $D_{bulk} = 38 \pm 2$ $\mu m^2/s$ (Ave. ± S.D., $N = 25$); (f) $\alpha_{bulk} = 0.82 \pm 0.04$ (Ave. ± S.D., $N = 14$); (g) $D_{\alpha, bulk} = 18 \pm 2$ $\mu m^2/s$ (Ave. ± S.D., $N = 14$) for $\alpha_{bulk} = 0.82$. Insets of (e, g) are D values for $\alpha = 1$ in droplets containing a pure buffer (control). Inset of (e) is reprinted from ref 27. Copyright 2021 American Chemical Society. Inset of (g) is reprinted from ref 25. Copyright 2020 American Chemical Society.

mixed one-phase regime.[14,15] Based on those observations, we hypothesized that even in the one-phase regime, spatial heterogeneity can emerge in single-component solutions of polydisperse polymers confined in small droplets owing to the length-dependent membrane wetting of polymers.[16,17]

To verify this hypothesis, we study concentrated solutions of dextran polymers confined in small droplets using experiments and simulations. We determine the spatial distribution of dextran chains near the droplet surface for various dispersities in length and analyze the diffusion of small molecules near the center of the droplets. This situation resembles the macromolecular crowding in cell nuclei, where long DNA and chromatin macromolecules surround small molecules, such as proteins.[18] We expect that the small molecules passing through the overlapped polymer chains change their diffusion according to the local distribution of the polymer chains.

As illustrated in Figure 1, we analyzed the molecular diffusion inside W/O droplets covered with a phosphatidylcholine (PC) lipid membrane, where 400 mg/mL dextran with a molecular weight of M_w = 150k (Dex150k) was confined. The estimated mesh size ξ (or correlation length) of the dextran solution is in the range of 1.9–2.4 nm (Sections S1 and S2). It is known that the transport of particles with radius r through polymer chains strongly depends on the size ratio, $2r/\xi$ (Figure 1b).[19−23] For $2r \ll \xi$, which can be achieved for small particles or low polymer concentrations, the particle diffusivities are expected to be similar to those in a pure solvent. However, for $2r \gg \xi$, the particle diffusivities should scale as $(2r/\xi)^{-2}$, according to scaling theory.[24] In the intermediate regime, $2r \approx \xi$, the particles and polymer segments frequently collide before they can fully relax, resulting in strong coupling with subdiffusive behavior at intermediate times. To cover a broad $2r/\xi$ regime, we chose two diffusive molecules: green fluorescent protein (GFP) with $2r$ = 5.6 nm[25] and 5-carboxytetramethylrhodamine (TAMRA) with $2r$ = 1.7 nm.[26]

First, we measured the diffusion of the TAMRA molecules ($2r/\xi$ = 0.7–0.9) by using fluorescence correlation spectroscopy (FCS). Figure 1c shows the typical autocorrelation functions (ACFs, $G(\tau)$) inside the droplets and in the bulk, revealing that the TAMRA diffusion inside a small droplet with R = 13 μm slows down compared to that in a large droplet with R = 58 μm and in the bulk. To evaluate the observed R-dependent diffusion, we fitted the fractional Brownian motion (fBM) equation to the ACFs measured inside the droplets with different R values (Section S1). The values of the obtained anomalous exponent α are plotted against R in Figure 1d; they are almost the same as the bulk value of $\alpha_{bulk} = 0.94 \pm 0.02$ (average value (Ave.) ± standard deviation (S.D.), sample

https://doi.org/10.1021/acsmaterialsau.3c00018
ACS Mater. Au 2023, 3, 442–449

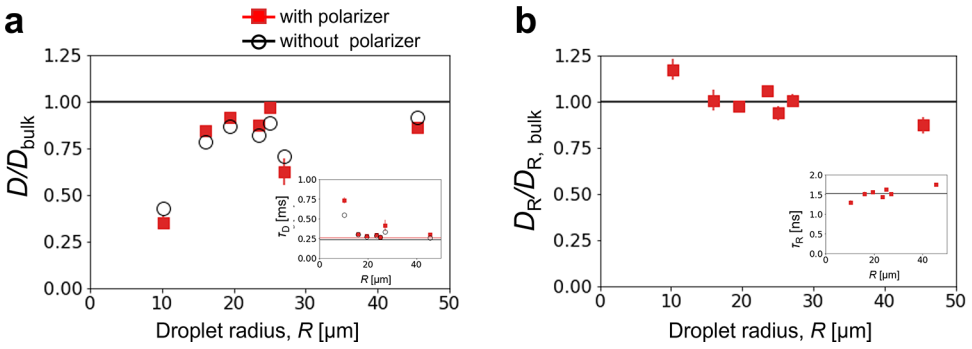

Figure 2. Droplet radius R dependence of (a) normalized translational diffusion coefficient, D/D_{bulk}, and (b) normalized rotational diffusion coefficient, $D_R/D_{R,bulk}$, of R6G inside 400 mg/mL dextran droplets using excitation light with polarizers (closed red squares) and without polarizers (open black circles). The insets show the R dependence of the (a) translational decay time, τ_D, and (b) rotational decay time, τ_R. The horizontal line shows their corresponding bulk values: (a) translational time analyzed with or without polarizers, $\tau_D = 0.26 \pm 0.01$ ms (Ave. ± standard error (S.E.), $N = 3$) and 0.234 ± 0.005 ms (Ave. ± S.E., $N = 6$), and (b) rotational time analyzed with polarizers, $\tau_R = 0.90 \pm 0.01$ ns (Ave. ± S.E., $N = 3$).

number $N = 25$), regardless of R. This slightly subdiffusive behavior is in very good agreement with that observed in previous simulations of colloid−polymer bulk mixtures, where a value of $\alpha_{bulk} = 0.98 \pm 0.01$ was found for $2r/\xi = 0.7$.[19] It means that the diffusion mode of TAMRA in the dextran solution is almost Brownian at any droplet size examined. We also derived the long-time diffusion coefficient, D, from the same data assuming normal diffusion ($\alpha = 1$) and normalized it by the bulk value, D_{bulk}, of 38 ± 2 $\mu m^2/s$ (Ave. ± S.D., $N = 25$) (Figure 1e). Contrary to the R-independent α, D/D_{bulk} decreases as R decreases below ∼20 μm, as previously reported.[27] This slow translational diffusion of TAMRA inside small droplets was not observed for droplets without dextran (the inset of Figure 1e). In addition, the TAMRA diffusion coefficient at low dextran concentrations with $2r \ll \xi$ is consistent with that without dextran (see Table S3 for the values and Figure S6d for ACFs.). These results agreed with our previous reports on TAMRA and Rhodamine 6G (R6G),[27] R6G in droplets containing linear polymer polyethylene glycol (PEG), and GFP in droplets containing bovine serum albumin.[25] Therefore, the observed R-dependent slow diffusion is a phenomenon that occurs inside small droplets crowded with polymers, regardless of the types of macromolecular crowder and tracer molecules.

Next, we measured the diffusion of GFP ($2r/\xi = 2.3$−2.9) inside the droplets. The examples of ACFs are shown in Figure S6a. The GFP molecules exhibit a much stronger subdiffusive behavior both in the bulk ($\alpha_{bulk} = 0.82 \pm 0.04$ (Ave. ± S.D., $N = 14$)) and in the droplets with any R (Figure 1f), which agrees with previous simulations where a value of $\alpha_{bulk} = 0.79 \pm 0.01$ was reported for $2r/\xi = 2.7$ in bulk solutions.[19] Focusing on the small droplets with $R < 20$ μm, there is a slight decrease in both α and D_α with decreasing R (Figure 1f,g), but the R dependence of D_α is significantly weaker than that of TAMRA (Figure 1e). These results mean that GFP molecules are much more strongly trapped in the dextran chains compared with the TAMRA molecules, which is consistent with the increase in $2r/\xi$. In our previous report, we confirmed that crowder polymers also exhibit R-dependent slow diffusion inside small droplets containing concentrated polymer solutions.[25] Therefore, the strong coupling between GFP and polymer chains may have caused the distribution of the distance traveled by the GFP to become non-Gaussian with a long tail, such that α and D fall with a decrease in R, where the polymer relaxation is also slowed.[28,29]

Unlike GFP, TAMRA exhibits R-dependent slow translational diffusion while maintaining $\alpha \sim 1$. A possible cause of the R-dependent slow diffusion is the increase in the tracer radius, r, due to the clustering of TAMRA molecules induced by the cell-sized confinement. To verify this hypothesis, we analyzed the rotational diffusion coefficient, D_R, which is expected to significantly decrease with an increase in r as $D_R \sim 1/\eta r^3$ based on the Stokes−Einstein−Debye equation, where η is the viscosity of the solution.[30] For this experiment, we need to separate the contributions of the translational and rotational diffusions, such that the translational decay time, τ_D, should be considerably longer than the rotational decay time, τ_R. We used the tracer molecule, R6G, for this rotational diffusion analysis since R6G has a similar size as TAMRA ($2r_{TAMRA} = 1.7$ nm ∼ $2r_{R6G} = 1.5$ nm), and reference values have been reported[31] for R6G but not for TAMRA.

Prior to the D_R analysis inside dextran droplets, we confirmed that the effect of polarization of the excitation light is negligible in the diffusion measurements from the almost identical translational correlation time, τ_D, in the bulk with or without the use of polarizers (Table S1 and Section S1). In addition, the values of the lifetime of the fluorescence molecule τ_L and of τ_R in the bulk without dextran are almost identical with the reference values.[32] Accordingly, we obtained τ_D inside the dextran droplets and plotted the normalized diffusion coefficients, D/D_{bulk}, against R for systems with and without polarizers (Figure 2a). We again observe a slow translational diffusion of R6G inside small dextran droplets with $R < 20$ μm, as in the case of TAMRA (Figure 1e).

Accordingly, we evaluate the D_R inside the dextran droplets based on the bulk values (Table S1). The resulting R dependence of τ_R and normalized $D_R/D_{R,bulk}$ are shown in Figure 2b. Even for small dextran droplets with $R < 20$ μm, which exhibit strongly slowed translational diffusion, $D_R/D_{R,bulk}$ is independent of R, maintaining a value almost equal to that in larger droplets and the bulk. This result suggests that the size of the tracer molecule, r, is essentially constant even for small droplets containing a highly concentrated dextran solution. Subsequently, we discuss why D_R appears to have increased for small droplets with $R = 10$ μm.

https://doi.org/10.1021/acsmaterialsau.3c00018
ACS Mater. Au 2023, 3, 442−449

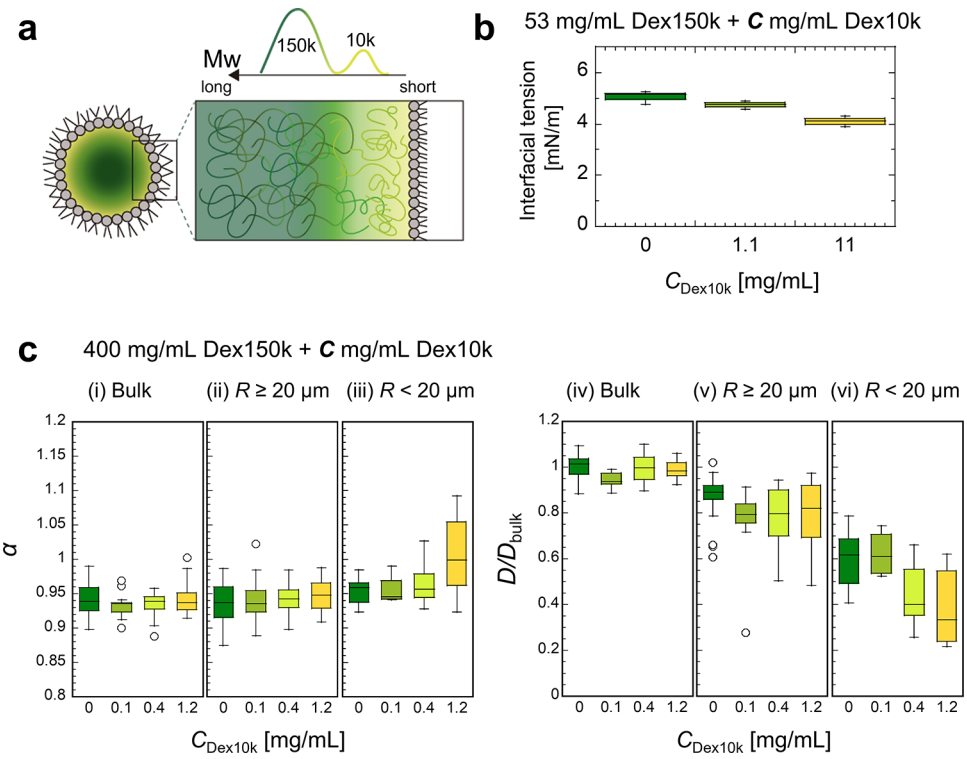

Figure 3. (a) Illustration of confinement-induced heterogeneous length distribution of dextran polymers. (b) Interfacial tension at the surface of droplets containing 53 mg/mL Dex150k without/with the addition of 1.1 or 11 mg/mL short Dex10k. (c) Anomalous exponent α (i-iii) and normalized diffusion coefficient D/D_{bulk} of TAMRA (iv–vi) of the bulk (i, iv), of large droplets with $R \geq 20$ μm (ii, v), and small droplets with $R <$ 20 μm (iii, vi) of 400 mg/mL Dex150k containing different concentrations of Dex10k (from left to right: 0, 0.1, 0.4, and 1.2 mg/mL). D_{bulk} represents the D of TAMRA in a bulk solution of 400 mg/mL Dex150k without Dex10k (the same data shown in Figure 1e). The error bars are SD. The numbers of trials (N) corresponding to the added dextran concentrations (0, 0.1, 0.4, and 1.2 mg/mL) were 25, 13, 21, and 15 (for the bulk); 27, 18, 18, and 20 (for $R > 20$ μm); 13, 4, 11, and 8 (for $R < 20$ μm).

CHAIN-LENGTH POLYDISPERSITY ENHANCES SLOW DIFFUSION

Next, we consider if the heterogeneous distribution of dextran chains inside the cell-sized droplets was the cause of the R-dependent slow translational diffusion of TAMRA. We expect that the higher M_w dextran chains are near the center of the droplet because of their lower wettability, ultimately inhibiting molecular transport in that region because of their higher viscosity and smaller mesh size, ξ.

Based on this hypothesis, we added shorter Dex10k polymers to the Dex150k solutions, expecting an enhanced localization of longer dextran chains at the droplet center, which should significantly decrease the D of TAMRA inside the small droplets, as illustrated in Figure 3a. Although the fluorescence labeling of Dex10k and Dex150k indicates a uniform distribution of dextran chain lengths inside the droplets (Figure S2), the polymer chain lengths may still be inhomogeneously distributed at scales smaller than the resolution of fluorescence microscopy. To confirm that the shorter Dex10k has a higher membrane wettability than Dex150k, the interfacial tension at the droplet surface, γ, was measured using the pendant drop method (Section S1). Owing to the difficulty in analyzing the γ for droplets containing a highly viscous solution of 400 mg/mL Dex150k, we analyzed the relaxation process for dextran droplets containing 53 mg/mL Dex150k and investigated the effects of adding shorter Dex10k chains at concentrations, C_{Dex10k}, of 1.1 and 11 mg/mL (Figure S3). As shown in Figure 3b, an increase in C_{Dex10k} lowered γ, showing that the shorter Dex10k indeed has a higher membrane wettability than Dex150k, as expected.

To establish a reference, we first analyzed the anomalous exponent, α, and the diffusion coefficient, D, of the bulk solutions of a 400 mg/mL Dex150k solution with small amounts of Dex10k (0.1, 0.4, and 1.2 mg/mL) (<0.5 wt % of total dextran). As shown in Figure 3c, i, iv, these small additions of short Dex10k did not alter the α or D of the bulk solutions. We also confirmed that the solution viscosity was maintained by the addition of 1.2 mg/mL Dex10k (Table S2). Next, the dextran solutions were confined in droplets, and we measured α and D/D_{bulk} against the droplet radius, R, where D_{bulk} is the diffusion coefficient of TAMRA in a bulk solution of 400 mg/mL Dex150k without adding shorter Dex10k (the same data shown in Figure 1e). Examples of their ACFs are shown in Figure S6b,c. The R dependence of α and D/D_{bulk} is shown in Figure S4. To visualize the effect of the addition of Dex10k, we combined the data of $R \geq 20$ μm and $R < 20$ μm and plotted them against the concentration of Dex10k, C_{Dex10k} (Figure 3c). For α, the trend of the droplets is similar to that of the bulk; i.e., α is almost unity independent of R and C_{Dex10k} (Figure 3c, ii–iii). In contrast, D/D_{bulk} is less than unity for droplets with any R (Figure 3c, v–vi). The decay of D/D_{bulk} with increasing C_{Dex10k} becomes particularly pronounced for small droplets with $R < 20$ μm, where it reaches less than half of the bulk value ($D/D_{bulk} < 0.5$).

These results strongly support the hypothesis that the slow translational diffusion of TAMRA ($2r/\xi \approx 0.7$–0.9) inside dextran droplets with $R < 20$ μm originates from the M_w-

https://doi.org/10.1021/acsmaterialsau.3c00018
ACS Mater. Au 2023, 3, 442–449

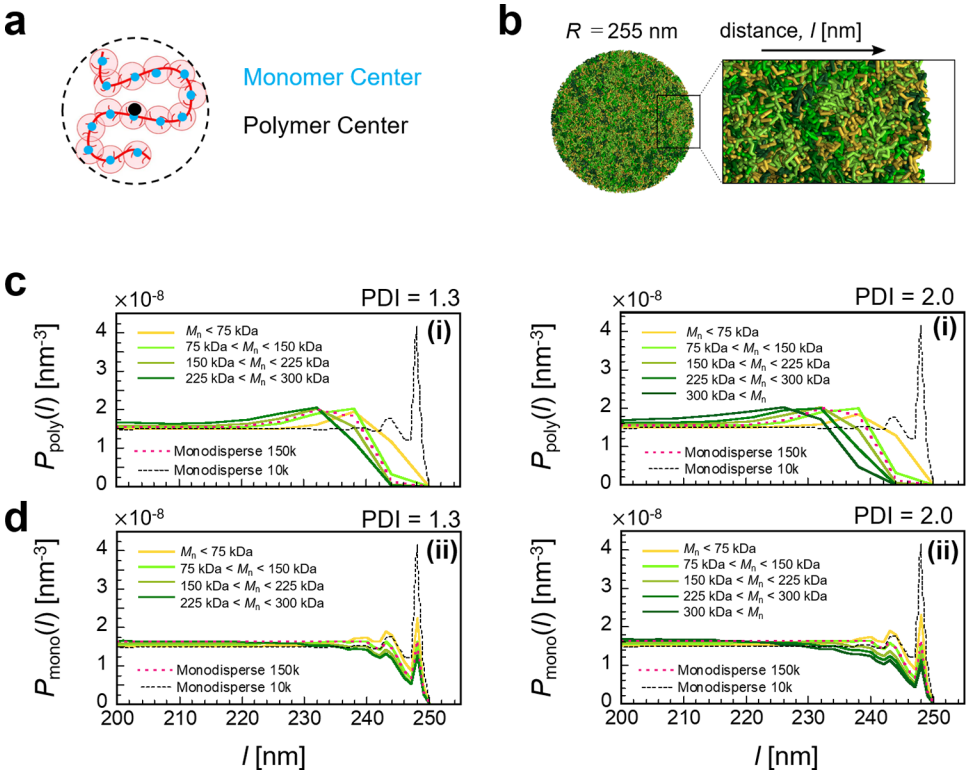

Figure 4. (a) Schematic representations of the model for a dextran chain (e.g., a chain of 14 beads). (b) Cross-sectional simulation snapshot of a dextran droplet with PDI = 2.0; chains are colored according to their molecular weight as in (c, d). (c, d) Probability distribution of finding a (c) monomer P_{mono} (l) or (d) polymer P_{poly} (l) at distance l from the droplet center for polydisperse solutions with PDI = 1.3 and 2.0 (data for PDI = 1.6 is shown in Figure S5). The red dotted and black dashed lines show the data of a monodisperse solution (PDI = 1.0) for Dex150k and Dex10k, respectively.

dependent (or length-dependent) membrane wetting of dextran polymers. Short and long polymers were preferentially distributed on the droplet surface and at the center, respectively.

HETEROGENEOUS DISTRIBUTION BY CHAIN LENGTH INSIDE DROPLETS

To study the distribution and conformation of the confined polymers with a molecular-level resolution, we performed dissipative particle dynamics (DPD) simulations of Dex150k and Dex10k mixtures confined in spherical droplets. Here, we used a similar model as in our recent computational study on PEG−dextran mixtures,[15] and we refer the reader to ref 15 and Section S3 for technical details. In this model, each Dex150k polymer is represented by a linear chain of 28 spherical beads connected by harmonic springs (an example of a polymer chain comprising 14 beads is shown in Figure 4a), whereas the Dex10k polymers are modeled as single beads. To mimic the good solubility of dextran in water, we set the Flory−Huggins interaction parameter to χ = 0 (the Dex10k chains are thus identical with the solvent beads in our model). We investigate solutions at four different conditions of dispersity, i.e., the polydispersity index (PDI; the ratio between M_w and number-average molecular weight, M_n) = 1.0, 1.3, 1.6, and 2.0, by drawing the lengths of the Dex150k chains from a Gaussian distribution. The monomer concentration of Dex150k was fixed at C = 30 wt % (~400 mg/mL). The droplet was modeled as a spherical container with radius R = 255 nm (Figure 4b). Although this size is approximately 40−200 times smaller than typical droplet sizes in experiments, the simulated droplets are large enough to capture the transition from the confinement-induced structuring near the droplet surface to the homogeneous distribution at the droplet interior, as demonstrated below.

In Figure 4c, we plot the probability distribution, P_{mono} (l), of finding a monomer at distance l from the droplet center for monodisperse solutions (PDI = 1.0) and solutions with different PDI values, i.e., (i) PDI = 1.3 and (ii) PDI = 2.0 (data for PDI = 1.6 are shown in Figure S5), itemized by molecular weight. The distribution of the monodisperse Dex150k case (PDI = 1.0) is shown as a red dotted line in each graph, while the distribution of Dex10k is shown as a black dashed line. These curves have been determined by averaging over 2000 independent simulation snapshots, and they have been normalized such that $\int_V P(l)\ dV = 1$ (the corresponding concentration profiles can be obtained by multiplying $P(l)$ with the number of monomers/polymers enclosed in the droplet, which are provided in Table S4). In all cases, we can identify a distinct layering of monomers near the droplet surface, which decays near $l \approx 235$ nm in the monodisperse case; the width of this layered region is approximately 25 nm, which is consistent with the characteristic diameter of the Dex150k chains in our simulations, i.e., $2R_g \approx 26$ nm. For polydisperse solutions, this zone becomes narrower/broader as the molecular weight decreases/increases relative to 150k, respectively. Comparing the curves of the different M_n windows, we can clearly see that the monomers from the shorter chains preferentially wet the droplet surface, which is consistent with smaller conformational entropy loss of shorter chains than longer chains. Furthermore, this higher

https://doi.org/10.1021/acsmaterialsau.3c00018
ACS Mater. Au 2023, 3, 442−449

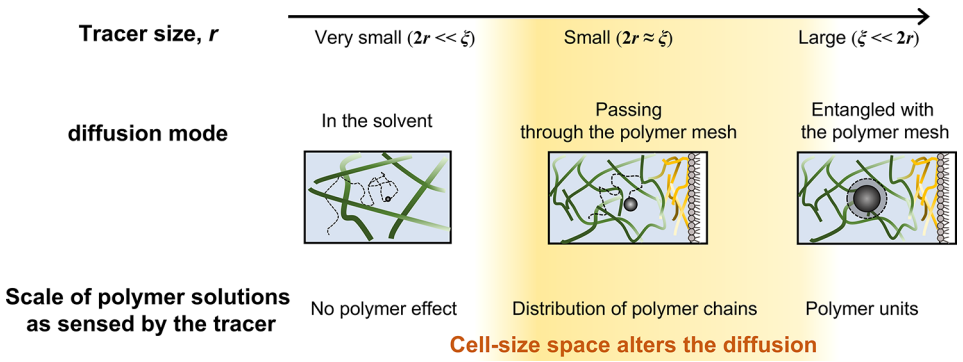

Figure 5. Possible mechanism of cell-sized space altering small-molecule diffusion through the polymer chains.

wettability of shorter chains agrees with that observed in interfacial tension data shown in Figure 3b. Owing to this preferential surface wetting of short dextran chains, there is a slight surplus of long dextran chains near the droplet center. Furthermore, if we compare the solutions with different PDI values, we discover that the differences in the $P(l)$ of the different M_n groups become slightly more pronounced with an increase in the PDI. After conducting the same analysis for the probability distribution of the polymer centers of masses, $P_{poly}(l)$, the same trends were observed (Figure 4d). Although our coarse-grained model provides invaluable insights into the confinement-induced structuring of the polymers by length, the soft nature of the interactions impedes a detailed analysis of the dynamics. To better understand these intricate dynamics, we are planning to perform additional simulations incorporating virtual slip-links between the DPD beads[33−35] or by employing a less coarse-grained model with our equilibrated configurations as a starting point.[36]

We demonstrated that the macromolecular crowding inside W/O droplets with a radius $R < 20$ μm caused a significant slowing down of the translational diffusion, D, of small tracer molecules (TAMRA, $2r/\xi \approx 0.7-0.9$) compared with that of large droplets and in the bulk, while the normalized rotational diffusion and anomalous exponent α remains almost unity. We rationalized this slow translational diffusion by the preferential wetting of short polymers at the droplet surface, which causes a surplus of long dextran chains at the droplet center (Figure 5). We hypothesize that the observed slow diffusion of tracer particles primarily originates from the strong coupling to the relaxations of polymer segments, which become significantly slower in confinement. Notably, a slight increase was observed in the rotational diffusion of TAMRA as the droplet radius decreased (Figure 2b). In addition, α appeared to approach unity with an increasing concentration of short Dex10k (Figure 3c, iii). These changes could be interpreted as a slight increase in ξ; however, this change in ξ was still sufficient to satisfy $2r/\xi \approx 1$, as observed for the size-dependent translational diffusion.

Although this R-dependent slow translational diffusion was not apparent for larger GFP tracer molecules ($2r/\xi \approx 2.3-2.9$), both α and D slightly fell with a decrease in R. This trend can be explained by the strong trapping of large GFP molecules by the confined polymer chains, where polymer relaxation was also slowed by cell-size confinement.[25] This R independence of large molecules is similar to the behavior of chromatin with a few micrometers in size as it diffuses through nuclei, following dynamic scaling regardless of the nuclear space size.[37] Therefore, the cell-sized confinement is likely a hidden parameter, which regulates molecular diffusion at intermediate length scales ($2r \approx \xi$), as shown in Figure 5.

The ability to control the spatial distribution of various polymers using differences in their surface wettability can be applied in various systems. For binary polymer blends of Dex70k and nongelling gelatin, the interfacial tension decreases with the addition of short dextran,[38] suggesting that the added short polymers are localized at the phase boundary to minimize the interfacial energy. Similarly, living cells have various surfaces, such as the cellular membrane, membrane organelle, and the surfaces of biomolecular condensates. Corresponding to this, the lengths of RNA and intrinsically disordered regions of RNA-binding proteins have been reported to be crucial for the emergence of LLPS and the physicochemical properties of the condensates.[39−41] Therefore, our findings on the wetting-induced heterogeneity of polymer chain length may contribute to the understanding of the heterogeneous distribution of molecules inside living cells.

EXPERIMENTAL SECTION

Experimental details are provided in Section S1.

ASSOCIATED CONTENT

Supporting Information

The Supporting Information is available free of charge at https://pubs.acs.org/doi/10.1021/acsmaterialsau.3c00018.

Materials and methods (Section S1), estimation of correlation length in the dextran solution (Section S2), molecular simulation model and method (Section S3), decay time of R6G in bulk solutions (Table S1), viscosity of dextran solutions (Table S2), diffusion coefficients of TAMRA in a solution without and with very low concentration Dex150k (Table S3), number of monomers/polymers in the simulations (Table S4), concentration dependence on the correlation length for dextran solution (Figure S1), fluorescence images of a dextran droplet (Figure S2), relaxation curves of interfacial tension γ on the surface of dextran droplets (Figure S3), droplet size dependence of TAMRA diffusion inside polydisperse dextran droplets (Figure S4), probability distribution of monomer or polymer against the distance from the droplet center (Figure S5), and examples of ACFs for GFP and TAMRA diffusion in dextran solutions (Figure S6) (PDF)

https://doi.org/10.1021/acsmaterialsau.3c00018
ACS Mater. Au 2023, 3, 442−449

AUTHOR INFORMATION

Corresponding Authors

Arash Nikoubashman − *Institute of Physics, Johannes Gutenberg University Mainz, 55128 Mainz, Germany; Department of Mechanical Engineering, Keio University, Kohoku, Yokohama 223-8522, Japan;* orcid.org/0000-0003-0563-825X; Email: anikouba@uni-mainz.de

Miho Yanagisawa − *Komaba Institute for Science, Graduate School of Arts and Sciences, The University of Tokyo, Meguro, Tokyo 153-8902, Japan; Graduate School of Science, The University of Tokyo, Bunkyo, Tokyo 113-0033, Japan; Center for Complex Systems Biology, Universal Biology Institute, The University of Tokyo, Meguro, Tokyo 153-8902, Japan;* orcid.org/0000-0001-7872-8286; Email: myanagisawa@g.ecc.u-tokyo.ac.jp

Authors

Yuki Kanakubo − *Komaba Institute for Science, Graduate School of Arts and Sciences, The University of Tokyo, Meguro, Tokyo 153-8902, Japan;* orcid.org/0009-0000-0347-1957

Chiho Watanabe − *School of Integrated Arts and Sciences, Graduate School of Integrated Sciences for Life, Hiroshima University, Higashi-Hiroshima 739-8521, Japan;* orcid.org/0000-0002-2114-3903

Johtaro Yamamoto − *Health and Medical Research Institute, National Institute of Advanced Industrial Science and Technology (AIST), Tsukuba, Ibaraki 305-8568, Japan;* orcid.org/0000-0002-6865-9069

Naoya Yanagisawa − *Komaba Institute for Science, Graduate School of Arts and Sciences, The University of Tokyo, Meguro, Tokyo 153-8902, Japan;* orcid.org/0000-0001-5748-4024

Hiroki Sakuta − *Komaba Institute for Science, Graduate School of Arts and Sciences, The University of Tokyo, Meguro, Tokyo 153-8902, Japan; Center for Complex Systems Biology, Universal Biology Institute, The University of Tokyo, Meguro, Tokyo 153-8902, Japan;* orcid.org/0000-0001-8473-6370

Complete contact information is available at: https://pubs.acs.org/10.1021/acsmaterialsau.3c00018

Author Contributions

CRediT: **Yuki Kanakubo** data curation (lead), formal analysis (lead), investigation (equal), validation (equal), writing-original draft (supporting), writing-review & editing (supporting); **Chiho Watanabe** formal analysis (equal), funding acquisition (supporting), validation (equal), visualization (lead), writing-original draft (equal), writing-review & editing (equal); **Johtaro Yamamoto** data curation (supporting), formal analysis (supporting), methodology (supporting), writing-review & editing (supporting); **Naoya Yanagisawa** data curation (supporting), formal analysis (supporting), writing-original draft (supporting), writing-review & editing (supporting); **Hiroki Sakuta** data curation (supporting), formal analysis (supporting), writing-review & editing (supporting); **Arash Nikoubashman** data curation (equal), formal analysis (equal), funding acquisition (equal), validation (equal), writing-original draft (equal), writing-review & editing (lead); **Miho Yanagisawa** conceptualization (lead), formal analysis (equal), funding acquisition (lead), project administration (lead), validation (equal), writing-original draft (lead), writing-review & editing (lead).

Notes

The authors declare no competing financial interest.

ACKNOWLEDGMENTS

We thank Prof. Kei Fujiwara (Keio University, Japan) for providing GFP samples. This research was funded by the Japan Society for the Promotion of Science (JSPS) KAKENHI (grant numbers 21H05871 and 22H01188 (M.Y.); 20K14425 (C.W.)), Japan Science and Technology Agency (JST) Program FOREST (JPMJFR213Y (M.Y.)), and ACT-X (JPMJAX191L (C.W.)). A.N. acknowledges funding provided by the Deutsche Forschungsgemeinschaft (DFG, German Research Foundation) through project number 470113688.

REFERENCES

(1) Zimmerman, S. B.; Trach, S. O. Estimation of macromolecule concentrations and excluded volume effects for the cytoplasm of Escherichia coli. *J. Mol. Biol.* **1991**, *222* (3), 599−620.

(2) Zhou, H. X.; Rivas, G.; Minton, A. P. Macromolecular crowding and confinement: biochemical, biophysical, and potential physiological consequences. *Annu. Rev. Biophys.* **2008**, *37*, 375−397.

(3) Lorenz, C.; Köster, S. Multiscale architecture: Mechanics of composite cytoskeletal networks. *Biophysics Reviews* **2022**, *3* (3), 031304.

(4) Riback, J. A.; Zhu, L.; Ferrolino, M. C.; Tolbert, M.; Mitrea, D. M.; Sanders, D. W.; Wei, M. T.; Kriwacki, R. W.; Brangwynne, C. P. Composition-dependent thermodynamics of intracellular phase separation. *Nature* **2020**, *581* (7807), 209−214.

(5) Pirone, D.; Lim, J.; Merola, F.; Miccio, L.; Mugnano, M.; Bianco, V.; Cimmino, F.; Visconte, F.; Montella, A.; Capasso, M.; et al. Stain-free identification of cell nuclei using tomographic phase microscopy in flow cytometry. *Nat. Photonics* **2022**, *16* (12), 851−859.

(6) Guo, S. M.; Yeh, L. H.; Folkesson, J.; Ivanov, I. E.; Krishnan, A. P.; Keefe, M. G.; Hashemi, E.; Shin, D.; Chhun, B. B.; Cho, N. H. Revealing architectural order with quantitative label-free imaging and deep learning. *eLife* **2020**, *9*, e55502 DOI: 10.7554/eLife.55502.

(7) Avni, A.; Joshi, A.; Walimbe, A.; Pattanashetty, S. G.; Mukhopadhyay, S. Single-droplet surface-enhanced Raman scattering decodes the molecular determinants of liquid-liquid phase separation. *Nat. Commun.* **2022**, *13* (1), 4378.

(8) Wang, Y.; Dai, W.; Liu, Z.; Liu, J.; Cheng, J.; Li, Y.; Li, X.; Hu, J.; Lu, J. Single-Cell Infrared Microspectroscopy Quantifies Dynamic Heterogeneity of Mesenchymal Stem Cells during Adipogenic Differentiation. *Anal. Chem.* **2021**, *93* (2), 671−676.

(9) Monterroso, B.; Zorrilla, S.; Sobrinos-Sanguino, M.; Keating, C. D.; Rivas, G. Microenvironments created by liquid-liquid phase transition control the dynamic distribution of bacterial division FtsZ protein. *Sci. Rep* **2016**, *6*, 35140.

(10) Hyman, A. A.; Weber, C. A.; Julicher, F. Liquid-liquid phase separation in biology. *Annu. Rev. Cell. Dev. Biol.* **2014**, *30*, 39−58.

(11) Boeynaems, S.; Alberti, S.; Fawzi, N. L.; Mittag, T.; Polymenidou, M.; Rousseau, F.; Schymkowitz, J.; Shorter, J.; Wolozin, B.; Van Den Bosch, L.; et al. Protein Phase Separation: A New Phase in Cell Biology. *Trends Cell Biol.* **2018**, *28* (6), 420−435.

(12) Fischer, T. M. A method to prepare isotonic dextran-salt solutions. *Cytometry A* **2010**, *77* (8), 805−810.

(13) Yanagisawa, M.; Watanabe, C.; Yoshinaga, N.; Fujiwara, K. Cell-Size Space Regulates the Behavior of Confined Polymers: From Nano- and Micromaterials Science to Biology. *Langmuir* **2022**, *38* (39), 11811−11827.

(14) Watanabe, C.; Furuki, T.; Kanakubo, Y.; Kanie, F.; Koyanagi, K.; Takeshita, J.; Yanagisawa, M. Cell-Sized Confinement Initiates Phase Separation of Polymer Blends and Promotes Fractionation upon Competitive Membrane Wetting. *ACS Mater. Lett.* **2022**, *4*, 1742−1748.

(15) Nikoubashman, A.; Yanagisawa, M. Confinement-Induced Fractionation and Liquid−Liquid Phase Separation of Polymer Mixtures. *Polymers* **2023**, *15* (3), 511.
(16) Silmore, K. S.; Howard, M. P.; Panagiotopoulos, A. Z. Vapour−liquid phase equilibrium and surface tension of fully flexible Lennard−Jones chains. *Mol. Phys.* **2017**, *115* (3), 320−327.
(17) Midya, J.; Egorov, S. A.; Binder, K.; Nikoubashman, A. Wetting transitions of polymer solutions: Effects of chain length and chain stiffness. *J. Chem. Phys.* **2022**, *156* (4), 044901.
(18) Miyoshi, D.; Sugimoto, N. Molecular crowding effects on structure and stability of DNA. *Biochimie* **2008**, *90* (7), 1040−1051.
(19) Chen, R.; Poling-Skutvik, R.; Nikoubashman, A.; Howard, M. P.; Conrad, J. C.; Palmer, J. C. Coupling of Nanoparticle Dynamics to Polymer Center-of-Mass Motion in Semidilute Polymer Solutions. *Macromolecules* **2018**, *51* (5), 1865−1872.
(20) Cai, L. H.; Panyukov, S.; Rubinstein, M. Mobility of Nonsticky Nanoparticles in Polymer Liquids. *Macromolecules* **2011**, *44* (19), 7853−7863.
(21) Chen, A.; Zhao, N.; Hou, Z. The effect of hydrodynamic interactions on nanoparticle diffusion in polymer solutions: a multiparticle collision dynamics study. *Soft Matter* **2017**, *13* (45), 8625−8635.
(22) Poling-Skutvik, R.; Krishnamoorti, R.; Conrad, J. C. Size-Dependent Dynamics of Nanoparticles in Unentangled Polyelectrolyte Solutions. *ACS Macro Lett.* **2015**, *4* (10), 1169−1173.
(23) Chen, R.; Poling-Skutvik, R.; Howard, M. P.; Nikoubashman, A.; Egorov, S. A.; Conrad, J. C.; Palmer, J. C. Influence of polymer flexibility on nanoparticle dynamics in semidilute solutions. *Soft Matter* **2019**, *15* (6), 1260−1268.
(24) Kalwarczyk, T.; Sozanski, K.; Ochab-Marcinek, A.; Szymanski, J.; Tabaka, M.; Hou, S.; Holyst, R. Motion of nanoprobes in complex liquids within the framework of the length-scale dependent viscosity model. *Adv. Colloid Interface Sci.* **2015**, *223*, 55−63.
(25) Watanabe, C.; Kobori, Y.; Yamamoto, J.; Kinjo, M.; Yanagisawa, M. Quantitative Analysis of Membrane Surface and Small Confinement Effects on Molecular Diffusion. *J. Phys. Chem. B* **2020**, *124* (6), 1090−1098.
(26) Szymanski, J.; Patkowski, A.; Wilk, A.; Garstecki, P.; Holyst, R. Diffusion and viscosity in a crowded environment: from nano- to macroscale. *J. Phys. Chem. B* **2006**, *110* (51), 25593−25597.
(27) Harusawa, K.; Watanabe, C.; Kobori, Y.; Tomita, K.; Kitamura, A.; Kinjo, M.; Yanagisawa, M. Membrane Surface Modulates Slow Diffusion in Small Crowded Droplets. *Langmuir* **2021**, *37* (1), 437−444.
(28) Munoz-Gil, G.; Volpe, G.; Garcia-March, M. A.; Aghion, E.; Argun, A.; Hong, C. B.; Bland, T.; Bo, S.; Conejero, J. A.; Firbas, N.; et al. Objective comparison of methods to decode anomalous diffusion. *Nat. Commun.* **2021**, *12* (1), 6253.
(29) Vilk, O.; Aghion, E.; Avgar, T.; Beta, C.; Nagel, O.; Sabri, A.; Sarfati, R.; Schwartz, D. K.; Weiss, M.; Krapf, D. Unravelling the origins of anomalous diffusion: From molecules to migrating storks. *Phys. Rev. Res.* **2022**, *4* (3), 033055.
(30) Roos, M.; Ott, M.; Hofmann, M.; Link, S.; Rossler, E.; Balbach, J.; Krushelnitsky, A.; Saalwachter, K. Coupling and decoupling of rotational and translational diffusion of proteins under crowding conditions. *J. Am. Chem. Soc.* **2016**, *138* (32), 10365−10372.
(31) Bain, A. J.; Chandna, P.; Butcher, G.; Bryant, J. Picosecond polarized fluorescence studies of anisotropic fluid media. II. Experimental studies of molecular order and motion in jet aligned rhodamine 6G and resorufin solutions. *J. Chem. Phys.* **2000**, *112* (23), 10435−10449.
(32) Wazawa, T.; Morimoto, N.; Nagai, T.; Suzuki, M. Rotational motion of rhodamine 6G tethered to actin through oligo(ethylene glycol) linkers studied by frequency-domain fluorescence anisotropy. *Biophys. Physicobiol.* **2015**, *12*, 87−102.
(33) Langeloth, M.; Masubuchi, Y.; Bohm, M. C.; Muller-Plathe, F. Recovering the reptation dynamics of polymer melts in dissipative particle dynamics simulations via slip-springs. *J. Chem. Phys.* **2013**, *138* (10), 104907.
(34) Ramirez-Hernandez, A.; Detcheverry, F. A.; Peters, B. L.; Chappa, V. C.; Schweizer, K. S.; Muller, M.; de Pablo, J. J. Dynamical Simulations of Coarse Grain Polymeric Systems: Rouse and Entangled Dynamics. *Macromolecules* **2013**, *46* (15), 6287−6299.
(35) Nikoubashman, A.; Davis, R. L.; Michal, B. T.; Chaikin, P. M.; Register, R. A.; Panagiotopoulos, A. Z. Thin films of homopolymers and cylinder-forming diblock copolymers under shear. *ACS Nano* **2014**, *8* (8), 8015−8026.
(36) Ohkuma, T.; Kremer, K.; Daoulas, K. Equilibrating high-molecular-weight symmetric and miscible polymer blends with hierarchical back-mapping. *J. Phys.: Condens. Matter* **2018**, *30* (17), 174001.
(37) Yesbolatova, A. K.; Arai, R.; Sakaue, T.; Kimura, A. Formulation of Chromatin Mobility as a Function of Nuclear Size during C. elegans Embryogenesis Using Polymer Physics Theories. *Phys. Rev. Lett.* **2022**, *128* (17), 178101.
(38) Vis, M.; Blokhuis, E. M.; Erne, B. H.; Tromp, R. H.; Lekkerkerker, H. N. W. Interfacial Tension of Phase-Separated Polydisperse Mixed Polymer Solutions. *J. Phys. Chem. B* **2018**, *122* (13), 3354−3362.
(39) Roden, C.; Gladfelter, A. S. RNA contributions to the form and function of biomolecular condensates. *Nat. Rev. Mol. Cell Bio* **2021**, *22* (3), 183−195.
(40) Laghmach, R.; Alshareedah, I.; Pham, M.; Raju, M.; Banerjee, P. R.; Potoyan, D. A. RNA chain length and stoichiometry govern surface tension and stability of protein-RNA condensates. *iScience* **2022**, *25* (4), 104105.
(41) Dignon, G. L.; Zheng, W.; Best, R. B.; Kim, Y. C.; Mittal, J. Relation between single-molecule properties and phase behavior of intrinsically disordered proteins. *Proc. Natl. Acad. Sci. USA* **2018**, *115* (40), 9929−9934.

https://doi.org/10.1021/acsmaterialsau.3c00018
ACS Mater. Au 2023, 3, 442−449